

X-rays from the oxygen-type Wolf-Rayet binary WR30a

Svetozar A. Zhekov^{1*} and Stephen L. Skinner²

¹*Institute of Astronomy and National Astronomical Observatory, 72 Tsarigradsko Chaussee Blvd., Sofia 1784, Bulgaria*

²*CASA, University of Colorado, Boulder, CO 80309-0389, USA*

ABSTRACT

We present an analysis of *XMM-Newton* X-ray data of WR 30a (WO+O), a close massive binary that harbours an oxygen-rich Wolf-Rayet star. Its spectrum is characterized by the presence of two well-separated broad peaks, or ‘bumps’, one peaking at energies between 1 and 2 keV and the other between 5 and 7 keV. A two-component model is required to match the observed spectrum. The higher energy spectral peak is considerably more absorbed and dominates the X-ray luminosity. For the currently accepted distance of 7.77 kpc, the X-ray luminosity of WR 30a is $L_X > 10^{34}$ erg s^{−1}, making it one of the most X-ray luminous WR+O binary amongst those in the Galaxy with orbital periods less than ~ 20 d. The X-ray spectrum can be acceptably fitted using either thermal or nonthermal models, so the X-ray production mechanism is yet unclear.

Key words: stars: individual: WR 30a — stars: Wolf-Rayet — X-rays: stars.

1 INTRODUCTION

Wolf-Rayet (WR) stars are massive stars that have powerful winds and are losing mass at high rates ($\dot{M} \sim 10^{-5}$ M_⊙ yr^{−1}; $V_{\text{wind}} = 1000 - 5000$ km s^{−1}). Based on their optical spectra, they are divided into three subtypes: nitrogen-rich (WN), carbon-rich (WC), and oxygen-rich (WO). Their progenitors are massive stars with initial masses > 25 M_⊙ and most WR stars are thought to end their lives as supernovae (see Crowther 2007 for a review on the physical properties of WRs). The observed binary fraction in Galactic Wolf-Rayet stars is relatively high with about 40% being members of WR+O systems (van der Hucht 2001).

WR stars were discovered to be X-ray sources by the *Einstein Observatory* (Seward et al. 1979). The first systematic survey of WRs showed that WR+O binaries are the brightest X-ray sources amongst them (Pollock 1987). Their enhanced emission likely originates from the interaction region of the winds of the massive binary components (Prilutskii & Usov 1976; Cherepashchuk 1976).

After the launch of the modern X-ray observatories *Chandra* and *XMM-Newton*, the number of WR stars with good quality X-ray spectra has increased considerably. Thus, some similarities and differences in the characteristics of their X-ray emission are now established.

Most WR stars are classified as either WC or WN subtypes and analysis of undispersed spectra of presumably single objects have revealed clear differences between WC and WN stars. All observations of putatively single WC stars so far have resulted in non-detections (Oskinova et al. 2003;

Skinner et al. 2006). In contrast, WN stars without known companions are detected in X-rays and their spectra typically reveal an admixture of cool (kT < 1 keV) and hot (kT > 2 keV) plasma (Skinner et al. 2010, 2012). WO stars are much rarer. The only pointed X-ray observations of a presumably single Galactic WO star to date, WR 142, resulted in a detection (Oskinova et al. 2009; Sokal et al. 2010). Interestingly, the *Chandra* detection of WR 142 showed an extremely hard and heavily-absorbed X-ray spectrum which could be fitted using either thermal or nonthermal models (Sokal et al. 2010).

On the other hand, the X-ray properties of massive WR+O binaries do not seem to have any strong dependence on the subtype of the WR component. Analyses of the X-ray emission from both close and wide WR+O binaries give support to the idea that a substantial fraction of their X-ray emission arises in colliding stellar wind (CSW) shocks, resulting from the interaction of the massive winds of the binary components (e.g., Skinner et al. 2001; Raassen et al. 2003; Schild et al. 2004; Pollock et al. 2005; Zhekov & Park 2010a, b; Zhekov et al. 2011, 2014; Zhekov 2012). But no WR+O binary with an oxygen-rich WR component has heretofore been detected in X-rays.

In this paper, we report the X-ray detection of the close WO+O binary system WR 30a. The paper is organized as follows. We summarize information on WR 30a in Section 2. In Section 3, we review the X-ray observations and data. In Section 4, we present results from analysis of the X-ray properties of WR 30a. In Section 5, we discuss our results, and we present our conclusions in Section 6.

* E-mail: szhekov@astro.bas.bg; stephen.skinner@colorado.edu.

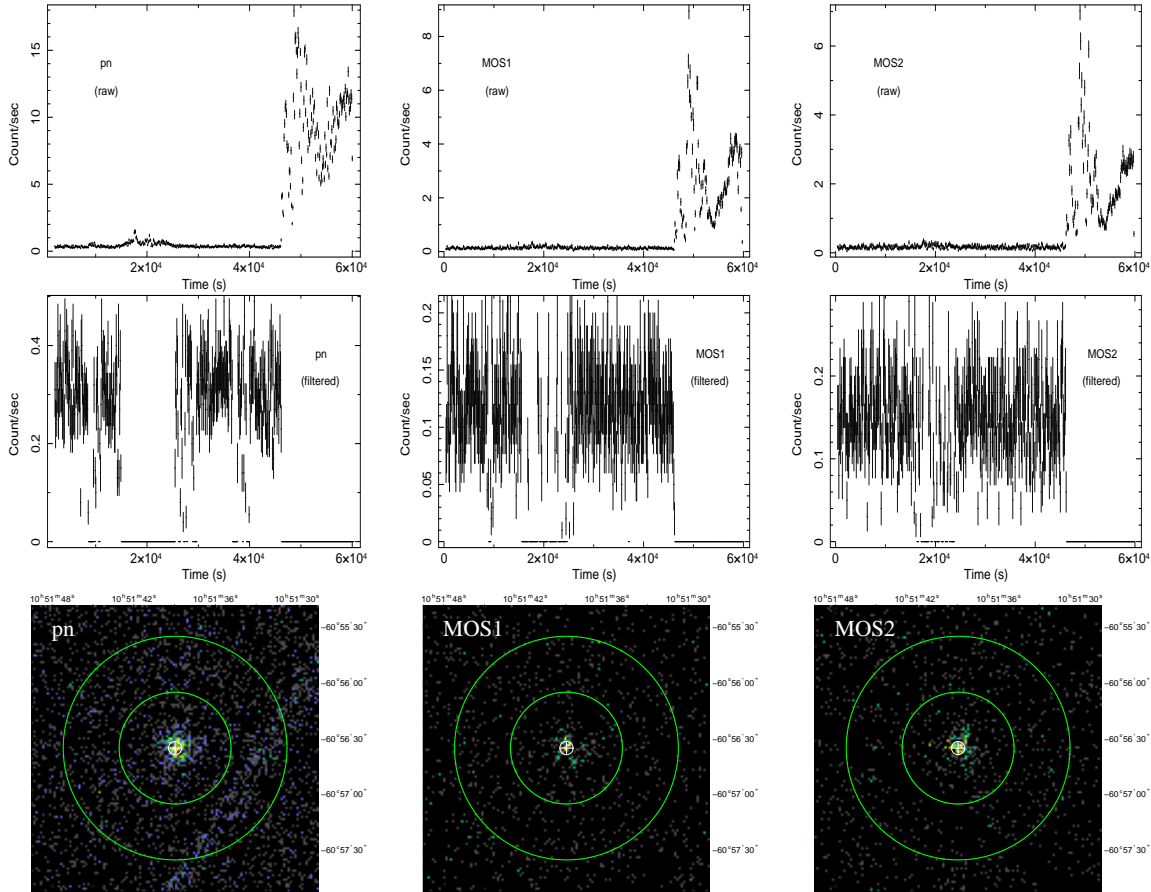


Figure 1. *Top row.* The total-field high-energy (>10 keV) EPIC light curves of WR 30a. *Middle row.* The total field high-energy EPIC light curves of WR 30a after being *filtered* to remove high X-ray background. *Bottom row.* The *filtered* EPIC images of WR 30a in the 0.2-10 keV energy band. The source spectrum was extracted from within the central circle (radius of $30''$). The background spectrum was extracted from the surrounding annulus (outer radius of $60''$). The circled plus sign gives the optical position of WR 30a (SIMBAD).

2 THE WOLF-RAYET STAR WR 30a

WR 30a (V574 Car; [MS70]) is one of four known oxygen-rich WR stars in the Galaxy (van der Hucht 2001, 2006; also Galactic Wolf-Rayet Catalogue¹). It is a WO4+O5-5.5 binary system at a distance of 7.77 kpc (van der Hucht 2001). Detailed photometric and spectroscopic studies proposed an orbital period of 4.619 d and classified the O5 component as either a main-sequence or, more likely, a giant star (Gosset et al. 2001). The optical extinction toward WR 30a is $A_v = 4.26$ mag (van der Hucht 2001; $A_v = 1.11 A_V$) implying a foreground column density of $N_H = (6.33 - 8.52) \times 10^{21} \text{ cm}^{-2}$. The range corresponds to the conversion that is used: $N_H = (1.6 - 1.7) \times 10^{21} A_V \text{ cm}^{-2}$ (Vuong et al. 2003, Getman et al. 2005); and $N_H = 2.22 \times 10^{21} A_V \text{ cm}^{-2}$ (Gorenstein 1975). Similarly to other WO stars, WR 30a has a very fast stellar wind: $V_{\text{wind}} = 4500 \text{ km s}^{-1}$ (Kingsburgh et al. 1995).

No radio data on WR 30a were found in the literature. Pollock et al. (1995) reported an X-ray non-detection in the

ROSAT PSPC Survey on Wolf-Rayet stars, likely due to the very short exposure time (260 s).

3 OBSERVATIONS AND DATA REDUCTION

We searched the *Chandra* and *XMM-Newton* archives for data on WR 30a and found one X-ray data set. WR 30a was observed with *XMM-Newton* on 2010 January 25 (Observation ID 0606330101) with a nominal exposure of ~ 60 ks. Our study is based on the data from the European Photon Imaging Camera (EPIC), which has one pn and two nearly-identical MOS detectors². We used the *XMM-Newton* SAS³ 14.0.0 data analysis software for data reduction, following the procedures summarized below.

First, the SAS pipeline processing scripts *emproc* and *epproc* were executed to incorporate the most recent calibration files (as of 2015 January 27). The data were checked for high X-ray background following the instructions in the SAS

² See § 3.3 in the *XMM-Newton* Users Handbook, Issue 2.12, 2014 (ESA: XMM-Newton SOC) http://xmm.esac.esa.int/external/xmm_user_support/documentation/uhb
³ Science Analysis Software, <http://xmm.esac.esa.int/sas>

¹ <http://pacrowther.staff.shef.ac.uk/WRcat/index.php>

documentation⁴, namely, by constructing total-field light curves at high energies: $E > 10$ keV for MOS1,2 and E in the 10 - 12 keV range for pn. As seen from Fig. 1, a high (and flaring) X-ray background was registered in the EPIC exposure, with the pn data being most affected. Nevertheless, we applied a background filtering procedure that allowed us to make use of some of the pn exposure and a substantial fraction of the MOS exposures.

We made use of the *XMM-Newton* Extended Source Analysis Software (XMM-ESAS) package⁵, which is now incorporated in SAS. We created filtered event files using the ESAS commands *mos-filter* and *pn-filter* which minimize the contamination of the soft proton flaring in the EPIC data in a robust manner (for details see the XMM-ESAS Cookbook⁶). As a check, we constructed the total-field filtered light curves at high energies (Fig. 1) which provided confidence that the background had been reduced to an acceptable level.

We then proceeded with the source and background spectral extraction from the pn and MOS1,2 filtered event files using the extraction regions shown in Fig. 1. The SAS procedures *rmfgen* and *arfgen* were used to generate the corresponding response matrix files and ancillary response files for each spectrum. The MOS spectrum used in our analysis is the sum of the spectra from the two MOS detectors. The extracted spectra (0.2 - 10 keV) of WR 30a had ~ 403 source counts (~ 710 source+background counts) in the 24.1-ks pn effective exposure and ~ 350 source counts (~ 584 source+background counts) in the 37.2-ks MOS effective exposure (36.0 ks in MOS1 and 38.4 ks in MOS2).

Since the pn exposure was more heavily affected by high X-ray background, our analysis emphasized the MOS spectrum while the pn spectrum was used to check the consistency of the results. For the spectral analysis, we used version 12.8.2 of XSPEC (Arnaud 1996).

Also, we constructed the pn and MOS1,2 background-subtracted light curves of WR 30a. Since the deleted high-background time intervals were unevenly-spaced, the good time intervals (GTIs) in the filtered light curves were as well. There were 27 GTI segments as short as 120 s and as long as 6,540 s in MOS1; 38 GTI segments as short as 120 s and as long as 4,315 s in MOS; and 26 GTI segments as short as 15 s and as long as 7,080 s in pn. On a timescale less than 24-37 ks, the X-ray light curves were statistically consistent with a constant count rate. A constant count rate model gives a goodness-of-fit ≥ 0.98 using χ^2 fitting.

4 RESULTS

As apparent from Fig. 2, the X-ray spectra are nearly featureless and are characterized by two broad peaks or ‘bumps’, one at lower energies (peaking between 1 and 2 keV) and another at higher energies (maximum emission between 5 and 7 keV). Other than a possible contribution from the Fe K complex near 6.67 keV, there are no bright spectral lines that would clearly indicate thermal emission.

We thus explored both thermal (optically-thin plasma) and non-thermal (power-law) models in XSPEC.

For the thermal models, we adopted typical WO star abundances from van der Hucht et al. (1986). The emission plasma components were subject to common X-ray absorption (model *wabs* in XSPEC) representative of the interstellar medium (ISM). Some additional absorption, as expected from the winds, was also required to acceptably fit the total spectrum. Typical WO star abundances were adopted for the wind absorption which was modeled using *phabs* model in XSPEC. Due to the rather low number of X-ray counts and absence of strong lines, all the abundances were kept fixed at their adopted values during fitting.

The one-component model subject only to ISM X-ray absorption did not provide a good fit to the observed MOS spectrum of WR 30a. The same was true for the two-component model when using the same ISM absorption for each component.

The two-component model with individual X-ray absorptions for each emission component gave a very good fit to the MOS spectrum. However, the best-fit plasma-temperature (or power-law index) values of the different emission components overlapped at the 1σ level. We thus adopted a common value for these parameters in the final model fits, which means that the spectral shape of the emission components was the same but the two components differed in their respective amounts of thermal plasma (or non-thermal emission) and in their X-ray absorptions. When exploring the cases with wind absorption, we kept the common ISM X-ray absorption fixed to the values that correspond to the optical extinction of WR 30a (Section 2). As an additional check of our global modelling, we fitted the MOS and pn spectra of WR 30a simultaneously by making use of the same models described above.

Table 1 and Fig. 2 present the corresponding results from the fits to the *XMM-Newton* spectra of WR 30a. The fit results can be briefly summarized as follows. Both thermal and non-thermal models are successful in reproducing the X-ray spectrum. In the case of thermal models, a relatively hot plasma ($kT > 2$ keV) is required to be present in the X-ray emitting region. The first emission component in the models is subject to X-ray absorption that is in general consistent with the optical extinction toward WR 30a, while the second emission component is more heavily absorbed. If we adopt a common ISM absorption for both emission components, then only the second component requires some additional wind absorption (see Models B and D in Table 1). For illustration of the results from the model fits with a common ISM absorption, we show only the case with the upper limit for the range of values that correspond to the optical extinction (Section 2). We note that if the lower limit for the ISM absorption was used, then the derived model parameters were within their respective 1σ confidence intervals.

The X-ray luminosity of WR 30a, $L_X > 10^{34}$ erg s⁻¹, is quite high when compared to other WR stars in the Galaxy. The more heavily absorbed component responsible for the observed emission in the 5 - 7 keV range dominates the total luminosity in the 0.5-10 keV energy band.

⁴ see § 4.4.4 in Users Guide to the XMM-Newton Science Analysis System, Issue 11.0, 2014 (ESA: XMM-Newton SOC); http://xmm.esac.esa.int/external/xmm_user_support/documentation/sas-usg/usg/

⁵ <http://xmm.esac.esa.int/sas/current/doc/esas>

⁶ <ftp://xmm.esac.esa.int/pub/xmm-esas/xmm-esas.pdf>

Table 1. Global Spectral Model Results

Parameter	← Thermal →				← Non-thermal →			
	MOS		MOS+pn		MOS		MOS+pn	
	model A	model B	model A	model B	model C	model D	model C	model D
χ^2/dof	13.1/23	19.7/23	45.4/58	46.4/58	13.6/23	19.9/23	41.1/58	45.8/58
$N_{H,1}$ (10^{22} cm^{-2})	$0.50^{+0.20}_{-0.16}$	0.852	$0.66^{+0.17}_{-0.16}$	0.852	$0.78^{+0.48}_{-0.33}$	0.852	$1.00^{+0.33}_{-0.26}$	0.852
$N_{H,2}$ (10^{22} cm^{-2})	$135^{+53.9}_{-34.5}$		$112^{+26.9}_{-20.5}$		$142^{+63.3}_{-39.7}$		$118^{+0.25}_{-0.16}$	
$N_{He,1}$ (10^{22} cm^{-2})		$0.00^{+...}_{-...}$		$0.00^{+...}_{-...}$		$0.00^{+0.01}_{-0.00}$		$0.00^{+0.01}_{-0.00}$
$N_{He,2}$ (10^{22} cm^{-2})		$0.11^{+0.02}_{-0.02}$		$0.11^{+0.02}_{-0.02}$		$0.09^{+0.02}_{-0.02}$		$0.09^{+0.02}_{-0.01}$
kT (keV)	$4.36^{+4.10}_{-1.33}$	$2.71^{+0.88}_{-0.63}$	$4.24^{+3.92}_{-1.22}$	$2.87^{+0.81}_{-0.50}$				
EM ₁ (10^{54} cm^{-3})	$0.20^{+0.04}_{-0.03}$	$0.21^{+0.03}_{-0.03}$	$0.22^{+0.03}_{-0.02}$	$0.22^{+0.03}_{-0.02}$				
EM ₂ (10^{54} cm^{-3})	$15.0^{+21.4}_{-8.33}$	$9.41^{+10.2}_{-4.20}$	$8.90^{+6.76}_{-3.83}$	$8.66^{+5.01}_{-3.23}$				
Γ_{pow}					$2.22^{+0.68}_{-0.54}$	$2.41^{+0.86}_{-0.22}$	$2.39^{+0.48}_{-0.42}$	$2.70^{+0.58}_{-0.49}$
norm _{pow,1} (10^{-4})					$0.25^{+0.28}_{-0.11}$	$0.29^{+0.44}_{-0.06}$	$0.32^{+0.22}_{-0.12}$	$2.70^{+0.58}_{-0.49}$
norm _{pow,2} (10^{-4})					$23.6^{+76.7}_{-17.2}$	$7.18^{+39.2}_{-2.87}$	$19.9^{+34.6}_{-12.0}$	$14.9^{+36.8}_{-9.80}$
F_X ($10^{-13} \text{ erg cm}^{-2} \text{ s}^{-1}$)	1.87 (60.0)	1.73 (40.5)	1.67 (36.2)	1.76 (37.0)	2.14 (97.9)	1.83 (27.5)	1.91 (75.2)	1.90 (50.1)
$F_{X,1}$ ($10^{-13} \text{ erg cm}^{-2} \text{ s}^{-1}$)	0.55 (0.79)	0.47 (0.88)	0.58 (0.87)	0.49 (0.91)	0.55 (1.01)	0.50 (1.06)	0.54 (1.19)	0.48 (1.40)
$\log L_X$ (erg s ⁻¹)	34.64	34.47	34.42	34.43	34.85	34.30	34.74	34.56
$\log L_{X,1}$ (erg s ⁻¹)	32.76	32.80	32.80	32.82	32.86	32.89	32.94	33.00

Note. Results from fits to the EPIC spectra of WR 30a. The labels MOS and MOS+pn denote which spectra were fitted. The XSPEC models are: *wabs * apec + wabs * apec* (Model A); *wabs * (phabs * apec + phabs * apec)* (Model B); *wabs * powerlaw + wabs * powerlaw* (Model C); *wabs * (phabs * powerlaw + phabs * powerlaw)* (Model D). Note that both model components have the same spectral shape (see text for details). Tabulated quantities are the neutral hydrogen absorption column density (N_H), helium absorption column density (N_{He}) for the ‘wind’ components, plasma temperature (kT), emission measure ($EM = \int n_e n_{He} dV$), photon power-law index (Γ_{pow}), power-law model normalization (norm_{pow}), the observed X-ray flux (F_X) in the 0.5 - 10 keV range followed in parentheses by the unabsorbed value and the X-ray luminosity (L_X). $F_{X,1}$ and $L_{X,1}$ denote the values for the first model component, peaking at lower energies. The abundances for the thermal models are those typical for the WO stars (by number: H = 0.00, He = 0.266, C = 0.213, N = 0.00, O = 0.497, Ne = 9.69×10^{-3} , Mg = 1.26×10^{-2} , Si = 6.73×10^{-4} , S = 1.47×10^{-4} , Fe = 3.69×10^{-4} ; van der Hucht et al. 1986). The values for the emission measure and the X-ray luminosity are for a reference distance of $d = 7.77$ kpc. Errors are the 1σ values from the fits.

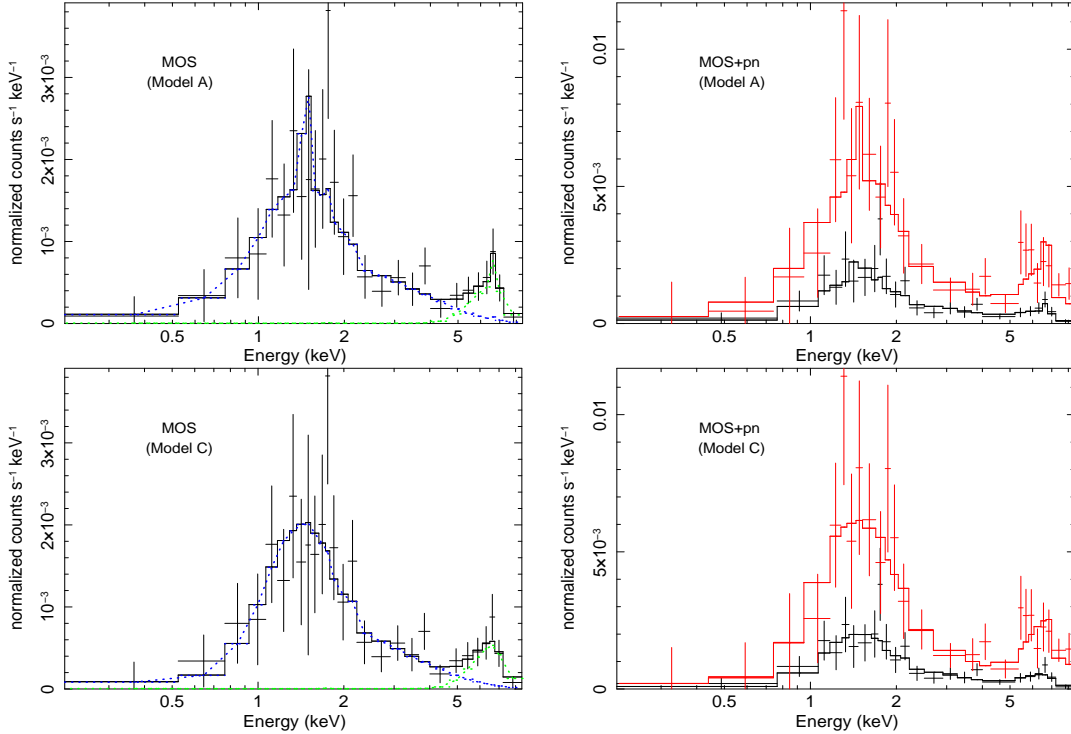


Figure 2. The background-subtracted EPIC spectra of WR 30a overlaid with some best-fitting models (Table 1). In the case of simultaneous fit to the MOS and pn spectra, the latter is plotted in red. For presentation purposes, the spectra were slightly re-binned with respect to the original binning of 20 counts per bin used in the fits. The model components are shown in blue and green colour.

5 DISCUSSION

Some of the results from the X-ray spectral fits may be affected by the fact that there are relatively few counts in the *XMM-Newton* spectra (Section 3). Nevertheless, the following physical picture emerges. There is likely some distribution of thermal X-ray plasma (or non-thermal emission) with similar plasma characteristics and this X-ray emission region is only partially absorbed. Alternatively, there may be two different X-ray sources with about the same plasma characteristics but one of them is more heavily absorbed. If the absorption is due to the stellar wind, that source must be located closer to the WO star while the other less-absorbed source is further from the star and is not subject to significant wind absorption.

If the X-rays from WR 30a are from CSW shocks in the WR+O binary, we expect a temperature-stratified interaction region. Thus, the derived values of the plasma temperature in our fits represent a mean temperature for the shocked plasma. For the case of typical WO abundances, the post-shock plasma temperature is $kT = 3.36 V_{1000}^2$ keV, where V_{1000} is the shock velocity in units of 1000 km s^{-1} . Given the stellar wind velocity of 4500 km s^{-1} (Section 2), high temperatures at $kT > 2$ keV are realistic for shocks in WO plasmas. Very high shock temperatures could be achieved even if the winds have not reached their terminal velocities before colliding, which could be the case in this close WO+O binary (orbital period of 4.619 d; Section 2).

Even though the high plasma temperatures ($kT > 2$ keV) determined from spectral fits could be taken as evidence for colliding stellar winds, it is worth keeping in mind that such high temperatures have also been detected in presumably single WN stars (Skinner et al. 2010, 2012) and in very close binaries like WR 46 (see Gosset et al. 2011; Zhekov 2012) and WR 155 (CQ Cep; see Skinner et al. 2015). So, CSWs may not be the only mechanism producing very hot plasma in WR stars.

However, as already noted, the spectral fits of WR 30a cannot clearly distinguish between thermal and nonthermal models. This ambiguity is due in part to the low number of spectral counts and higher signal-to-noise spectra capable of determining whether weak emission lines are present will be needed to discriminate between thermal and nonthermal emission. A similar ambiguity was found for the presumably single WO star WR 142 whose X-ray emission is even fainter and shows no strong lines (Sokal et al. 2010). WR 30a and WR 142 also reveal other similarities, e.g. both have a hard heavily-absorbed spectral component. A notable difference is that the X-ray luminosity of WR 142 is less than 1% of that of WR 30a. The binary nature of WR 30a may be largely responsible for this, but distance uncertainties could also contribute.

The X-ray luminosity of WR 30a ($L_X > 10^{34} \text{ erg s}^{-1}$, Table 1) may be the highest amongst the close WR+O binaries (orbital periods less than ~ 20 d) in the Galaxy studied so far (e.g., see Zhekov 2012; Skinner et al. 2015; Nazé et al. 2008), provided the adopted distance of 7.77 kpc is not significantly overestimated. The high X-ray luminosity must be accommodated by any plausible theoretical emission models.

We note that other close WR binaries with very high X-ray luminosities may exist in the Galaxy. Gagné et al. (2012)

have compiled a list of possible detections of colliding wind binaries with *Chandra*, *XMM-Newton* and *ROSAT*. High X-ray luminosity candidates are WR28, WR29, WR43a, WR43c and WR101k. However, caution is needed when considering the available data on these objects. For example, WR43a and WR43c are located in the core of the Galactic starburst region NGC 3603 and thus cannot be spatially resolved in X-rays (that is their X-ray spectra are contaminated by the near-by sources). Similarly, WR101k cannot be resolved since it is in the centre of the Galaxy only $1.8''$ from Sgr A (SIMBAD). The data on WR28 and WR29 are from *ROSAT* observations and only upper limits can be derived on their observed fluxes. Nevertheless, these close WR binaries which may have extremely high X-ray luminosities deserve more attention and in-depth X-ray studies.

Finally, a distinguishing feature of WR 30a is its unusual spectral shape with two broad separated peaks. After examining the X-ray spectra of other WR stars we were able to identify another object with a similarly shaped spectrum, the close WR+O binary WR 79.

5.1 Comparison with WR 79

WR 79 is a WC+O binary with an orbital period of 8.28 d at a distance of 1.99 kpc (van der Hucht 2001). Figure 3 compares its *Chandra* X-ray spectrum with that of WR 30a and WR 142. We note that WR 79 was also observed by *XMM-Newton* but its spectrum is contaminated by two nearby sources within $7'' - 8''$ that are seen in the higher spatial resolution *Chandra* image (for details, see Appendix A in Zhekov 2012).

Two broad peaks are present in both WR 79 and WR 30a, but only the higher energy peak is present in the apparently single WO star WR 142. No prominent spectral lines are seen with the possible exception of Fe emission in the 6-7 keV range in WR 79 and a hint of the same in WR 30a. But faint emission lines could be missed since the number of counts in all three spectra is quite limited, with only ~ 380 source counts in WR 79 (Zhekov 2012) and ~ 46 counts in WR 142 (Sokal et al. 2010).

The X-ray spectrum of WR 79 was well matched by a two-component optically-thin plasma model with individual wind absorptions (see Table 3 and Fig. 1 in Zhekov 2012). As the global fits showed, the second model component due to hot plasma with $kT > 2$ keV is subject to much higher wind absorption, which is also the case with WR 30a. And the more absorbed component, whose emission produces the broad peak between 4 and 7 keV in the spectrum, dominates the total luminosity in the 0.5-10 keV energy range. We did this estimate by making use of exactly the same spectral data (no re-processing) and models as in Zhekov (2012). Despite these similarities, there is an interesting difference: the X-ray luminosity of WR 79 is less than WR 30a by approximately one order of magnitude.

6 CONCLUSIONS

In this work, we presented and analyzed archival *XMM-Newton* data of WR 30a which provide the first X-ray spectra of this WR+O binary that harbours a rare oxygen-rich

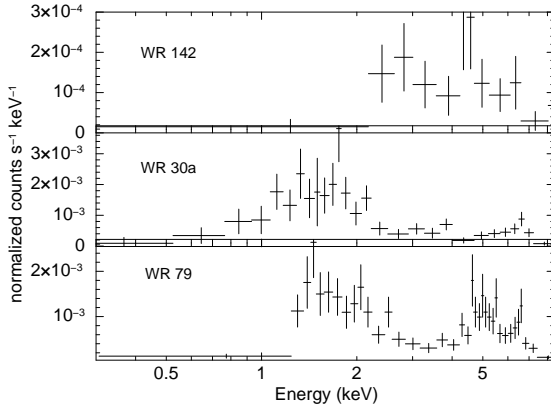


Figure 3. The background-subtracted spectra of WR 30a (*XMM-Newton* EPIC-MOS), WR 79 (*Chandra* ACIS-S, ObsId 5372, see Zhekov 2012) and WR 142 (*Chandra* ACIS-I, ObsId 9914; based on our own spectral extraction using version 4.7 of *Chandra* Interactive Analysis of Observations, CIAO; <http://cxc.harvard.edu/ciao/>).

Wolf-Rayet star. The main results and conclusions are as follows.

(i) The X-ray spectrum of WR 30a shows no strong spectral lines, although some Fe emission between 6 - 7 keV may be present and other weak lines may have been missed due to the low number of source counts in the spectrum. The spectrum can be acceptably fitted by either thermal or nonthermal emission models.

(ii) The most distinguishing feature in the WR 30a spectrum is the presence of two broad but well-separated peaks, one peaking at energies between 1 and 2 keV and the other between 5 and 7 keV. A two-component model is required to match the observed spectrum. The spectral component seen in the higher energy peak is considerably more absorbed and dominates the intrinsic X-ray luminosity in the 0.5-10 keV range.

(iii) For the currently accepted distance of 7.77 kpc, the X-ray luminosity of WR 30a is $L_X > 10^{34}$ erg s $^{-1}$, making it the most X-ray luminous object amongst the close WR+O binaries (orbital periods less than ~ 20 d) in the Galaxy studied so far.

(iv) On the basis of the double-peaked spectral shape and other X-ray characteristics, we have identified two WR binaries that are quite similar: WR 30a and WR 79 (WC+O).

(v) Future observations of both single and binary WO stars are needed to obtain higher signal-to-noise X-ray spectra capable of determining if faint emission lines are present and thereby distinguishing between thermal and nonthermal emission processes.

7 ACKNOWLEDGEMENTS

This research has made use of data and/or software provided by the High Energy Astrophysics Science Archive Research Center (HEASARC), which is a service of the Astrophysics Science Division at NASA/GSFC and the High Energy Astrophysics Division of the Smithsonian Astrophysical Observatory. This research has made use of the NASA's Astro-

physics Data System, and the SIMBAD astronomical data base, operated by CDS at Strasbourg, France. This work is based on observations obtained with XMM-Newton, an ESA science mission with instruments and contributions directly funded by ESA Member States and the USA (NASA).

REFERENCES

- Arnaud, K.A. 1996, in Jacoby G., Barnes, J. eds., ASP Conf. Ser. Vol. 101, *Astronomical Data Analysis Software and Systems*, Astron. Soc. Pac., San Francisco, 17
- Cherepashchuk, A.M. 1976, *Sov. Astron. Lett.*, 2, 138
- Crowther, P., 2007, *ARAA*, 45, 177
- Gagné, M., Fehon, G., Savoy, M.R., Cartagena, C.A., Cohen, D.H. & Owocki, S.P. 2012, *ASP Conference Series*, 465, 301
- Getman, K.V., Feigelson, E.D., Grosso, N., McCaughrean, M.J., Micela, G., Broos, P., Garmire, G., & Townsley, L. 2005, *ApJS*, 160, 363
- Gorenstein, P. 1975, *ApJ*, 198, 95
- Gosset, E., De Becker, M., Nazé, Y., Carpano, S., Rauw, G., Antokhin, I.I., Vreux, J.-M., & Pollock, A.M.T. 2011, *A&A*, 527, A66
- Gosset, E., Royer, P., Rauw, G., Manfroid, J. & Vreux, J.-M. 2001, *MNRAS*, 327, 425
- Kingsburgh, R.I., Barlow, M.J. & Torey, P.J. 1995, *A&A*, 295, 75
- Nazé, Y., Rauw, G. & Manfroid, J. 2008, *A&A*, 483, 171
- Oskinova, L.M., Ignace, R., Hamann, W.-R., Pollock, A.M.T., & Brown, J.C. 2003, *A&A*, 402, 755
- Oskinova, L.M., Hamann, W.-R., Feldmeier, A., Ignace, R. & Chu, Y.-H. 2009, *ApJ*, 693, L34
- Pollock, A.M.T. 1987, *ApJ*, 320, 283
- Pollock, A.M.T., Haberl, F., & Corcoran, M.F. 1995, in van der Hucht K.L., Williams P.M., eds. *Proc. IAU Symp 163, Wolf-Rayet Stars: Binaries, Colliding Winds, Evolution*, Kluwer, Dordrecht, p. 512
- Pollock, A.M.T., Corcoran, M.F., Stevens, I.R., & Williams, P.M. 2005, *ApJ*, 629, 482
- Prilutskii, O.F. & Usov, V.V. 1976, *SvA*, 20, 2
- Raassen, A.J.J., van der Hucht, K.A., Mewe, R., Antokhin, I.I., Rauw, G., Vreux, J.-M., Schmutz, W. & Güdel, M. 2003, *A&A*, 402, 653
- Schild, H. et al. 2004, *A&A*, 422, 177
- Seward, F., Forman, W.R., Giacconi, R., Griffiths, R.E., Harnden, F.R., Jones, C. & Pye, J.P. 1979, *ApJ*, 234, L55
- Skinner, S.L., Güdel, M., Schmutz, W. & Stevens, I.R. 2001, *ApJ*, 558, L113
- Skinner, S.L., Güdel, M., Schmutz, W. & Zhekov, S.A. 2006, *Ap&SS*, 304, 97
- Skinner S.L., Zhekov S.A., Güdel M. & Schmutz W. 2015, *ApJ*, 799, 124
- Skinner S.L., Zhekov S.A., Güdel M., Schmutz W. & Sokal, K.R. 2010, *AJ*, 139, 825
- Skinner S.L., Zhekov S.A., Güdel M., Schmutz W. & Sokal, K.R. 2012, *AJ*, 143, 116
- Sokal, K.R., Skinner S.L., Zhekov S.A., Güdel M. & Schmutz W. 2010, *ApJ*, 715, 1327
- van der Hucht, K.A. 2001, *NewAR*, 45, 135
- van der Hucht, K.A. 2006, *A&A*, 458, 453

- van der Hucht, K.A., Cassinelli, J.P., & Williams P.M.
1986, A&A, 168, 111
- Vuong, M.H., Montmerle, T., Grosso, N., Feigelson, E.D.,
Verstraete, L., & Ozawa, H. 2005, A&A, 408, 581
- Zhekov, S.A. 2012, MNRAS, 422, 1322
- Zhekov, S.A., Gagné, M. & Skinner, S.L. 2011, ApJ, 727,
L17
- Zhekov, S.A., Gagné, M. & Skinner, S.L. 2014, ApJ, 785,
8
- Zhekov S.A., & Park, S. 2010a, ApJ, 709, L119
- Zhekov S.A., & Park, S. 2010b, ApJ, 721, 518

This paper has been typeset from a \LaTeX file prepared
by the author.